

Article

# Zinc Donor–Acceptor Schiff Base Complexes as Thermally Activated Delayed Fluorescence Emitters

Andreas Russegger , Lisa Eiber, Andreas Steinegger and Sergey M. Borisov \*

Institute of Analytical Chemistry and Food Chemistry, Graz University of Technology, Stremayrgasse 9, 8010 Graz, Austria; russegger@tugraz.at (A.R.); lisa.eiber@gmx.at (L.E.); andreas.steinegger@tugraz.at (A.S.)

\* Correspondence: sergey.borisov@tugraz.at

**Abstract:** Four new zinc(II) Schiff base complexes with carbazole electron donor units and either a 2,3-pyrazinedicarbonitrile or a phthalonitrile acceptor unit were synthesized. The donor units are equipped with two bulky 2-ethylhexyl alkyl chains to increase the solubility of the complexes in organic solvents. Furthermore, the effect of an additional phenyl linker between donor and acceptor unit on the photophysical properties was investigated. Apart from prompt fluorescence, the Schiff base complexes show thermally activated delayed fluorescence (TADF) with quantum yields up to 47%. The dyes bearing a phthalonitrile acceptor emit in the green–yellow part of the electromagnetic spectrum and those with the stronger 2,3-pyrazinedicarbonitrile acceptor—in the orange–red part of the spectrum. The emission quantum yields decrease upon substitution of phthalonitrile with 2,3-pyrazinedicarbonitrile and upon introduction of the phenyl spacer. The TADF decay times vary between 130  $\mu$ s and 3.5 ms at ambient temperature. The weaker phthalonitrile acceptor and the additional phenyl linker favor longer TADF decay times. All the complexes show highly temperature-dependent TADF decay time (temperature coefficients above  $-3\%/K$  at ambient conditions) which makes them potentially suitable for application as molecular thermometers. Immobilized into cell-penetrating RL-100 nanoparticles, the best representative shows temperature coefficients of  $-5.4\%/K$  at 25 °C that makes the material interesting for further application in intracellular imaging.

**Keywords:** TADF; temperature; decay time; donor–acceptor; sensor



**Citation:** Russegger, A.; Eiber, L.; Steinegger, A.; Borisov, S.M. Zinc Donor–Acceptor Schiff Base Complexes as Thermally Activated Delayed Fluorescence Emitters.

*Chemosensors* **2022**, *10*, 91.  
<https://doi.org/10.3390/chemosensors10030091>

Academic Editors: Xudong Wang and Hongshang Peng

Received: 23 December 2021

Accepted: 22 February 2022

Published: 26 February 2022

**Publisher’s Note:** MDPI stays neutral with regard to jurisdictional claims in published maps and institutional affiliations.



**Copyright:** © 2022 by the authors. Licensee MDPI, Basel, Switzerland. This article is an open access article distributed under the terms and conditions of the Creative Commons Attribution (CC BY) license (<https://creativecommons.org/licenses/by/4.0/>).

## 1. Introduction

Temperature is one of the key parameters in daily life, industry and scientific research, and is quantified with temperature sensors. Commonly used temperature sensors can be divided into several groups, depending on which temperature-dependent physical parameter is measured: volume in a liquid-filled glass thermometer, electrical resistance in a resistance thermometer or voltage in case of a thermocouple, to mention the most common types. Despite being highly useful, these readily available sensors are not suitable for a number of important applications. Particularly, they cannot be used for measurements in very small objects such as (microfluidic) chips and living cells because their spatial resolution is limited to around 10  $\mu$ m [1]. Luminescent temperature probes [1–5] not only overcome the above limitation, but also allow 2D and 3D mapping of temperature distribution via imaging techniques.

The so-called “molecular thermometers” represent the first large group of optical probes. They rely on fluorescent dyes such as rhodamine derivatives [6,7], BODIPYs [8,9], perylenes [10,11], etc., phosphorescent complexes of transition metals (ruthenium(II) [12], iridium(III) [13], europium(III) [14,15], platinum(II) [16,17], palladium(II) [17], etc.) or stained polymeric probes [18,19] that utilize conformational changes of the material. Inorganic materials, including quantum dots [20,21], (upconverting) lanthanide nanoparticles [22], metal clusters [23,24] and phosphors [22,25,26], represent the second large class.

Purely organic dyes and metal complexes that emit thermally activated delayed fluorescence (TADF) have been extensively investigated in the last decade in context of application

in OLED technology [27,28]. Although optical temperature sensing with the help of TADF emitters was demonstrated a while ago [29,30], only recently have molecular thermometers on their basis attracted significant attention. Sensors utilizing TADF-emitting carbon dot-based nanocomposite [31], polymers based on 1,8-naphthalimide [32], anthraquinone and dicyanobenzene -derived [33] organic dyes, as well as Pt(II), Pd(II) and Zn(II) complexes with benzoporphyrins [34,35] have been reported.

Previously, we presented a new group of TADF emitters based on Zn(II) complexes with Schiff bases [36]. These dyes rely on an abundant metal and, in this respect, are comparable to metal-free TADF emitters. On the other hand, they feature particularly high molar absorption coefficients in the visible part of electromagnetic spectrum ( $39,000\text{--}75,000\text{ M}^{-1}\text{cm}^{-1}$ ) and are also characterized by high temperature sensitivity of the TADF decay time at ambient temperature ( $\sim\text{--}3.5\%/K$  for polymer-immobilized dyes). Among the two dyes investigated, the one with the carbazole electron donor featured a significantly higher ratio of TADF to prompt fluorescence and several-fold-shorter decay times compared to the analogue utilizing the dialkylaniline donor group, but, unfortunately, it also possessed poor solubility in organic solvents. Thus, it is of considerable interest to investigate a broader palette of the new emitters and improve the solubility of the dyes in organic solvents and polymers to minimize potential aggregation issues.

In this work, we present four Zn(II) Schiff base complexes that include a combination of a carbazole donor with two different acceptor units and optionally include a phenyl linker (Figure 1). It will be shown that the nature of the acceptor unit and presence of the linker strongly influence the photophysical properties of the dyes, whereas the temperature sensing characteristics are barely affected by the modifications.

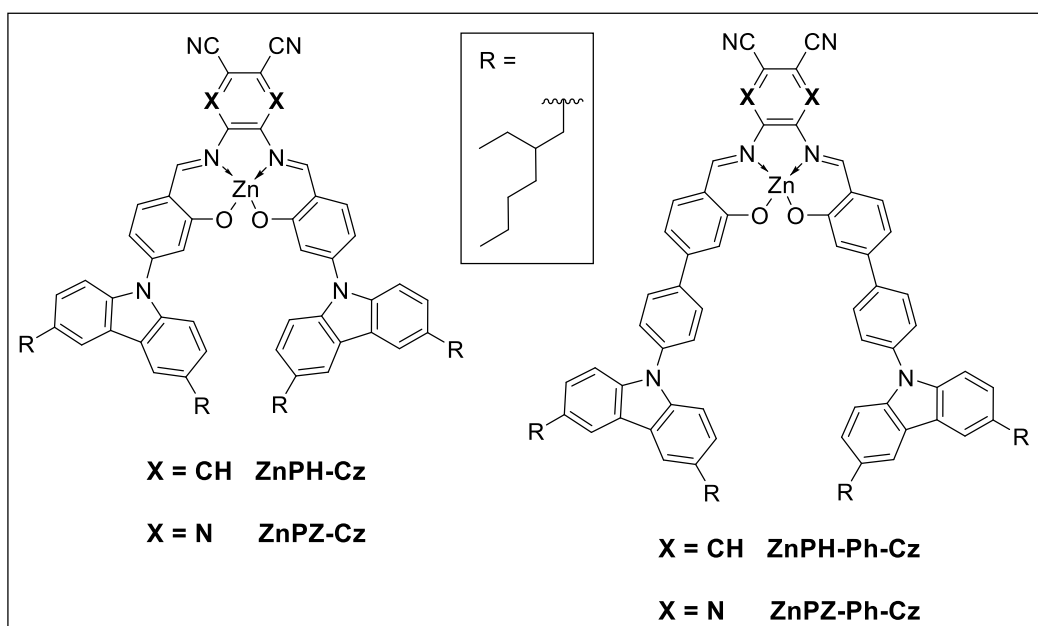


**Figure 1.** Structure of new Zn(II) Schiff base complexes.

## 2. Materials and Methods

### 2.1. Materials

9*H*-Carbazole, 4-bromo-2-methoxybenzaldehyde, 4-bromo-2-hydroxybenzaldehyde, 4,5-diaminophthalonitrile and tris(dibenzylideneacetone)dipalladium(0) ( $\text{Pd}_2(\text{dba})_3$ ) were purchased from Fluorochem ([www.fluorochem.co.uk](http://www.fluorochem.co.uk) (24 February 2022)), tri-*tert*-butylphosphonium tetrafluoroborate ( $[(t\text{-Bu})_3\text{PH}]\text{BF}_4$ ) was obtained from ABCR ([www.abcr.de](http://www.abcr.de) (24 February 2022)), dichloromethane (DCM) and pyridine (Py) were from Fisher Scientific ([www.fishersci.com](http://www.fishersci.com) (24 February 2022)). 2-Ethylhexanoyl chloride and 2-isopropoxy-4,4,5,5-tetramethyl-1,3,2-dioxaborolane were purchased from TCI Europe ([www.tcichemicals.com](http://www.tcichemicals.com) (24

February 2022)). Cesium carbonate ( $\text{Cs}_2\text{CO}_3$ ), boron tribromide dimethyl sulfide complex ( $\text{BBr}_3 \cdot \text{Me}_2\text{S}$ ), 5,6-diamino-2,3-pyrazinedicarbonitrile, zinc acetate dihydrate ( $\text{Zn}(\text{AcO})_2$ ), copper(I) iodide ( $\text{CuI}$ ), glucose oxidase from *Aspergillus niger* (~200 U/mg), D-(+)-glucose monohydrate were obtained from Sigma Aldrich ([www.sigmaaldrich.com](http://www.sigmaaldrich.com) (24 February 2022)). Dimethylformamide (DMF), tetrahydrofuran (THF), toluene (HPLC grade), anhydrous sodium sulfate ( $\text{Na}_2\text{SO}_4$ ) and sodium sulfite ( $\text{Na}_2\text{SO}_3$ ) were purchased from Carl Roth ([www.carlroth.com](http://www.carlroth.com) (24 February 2022)). Deuterated solvents were obtained from Eurisotop ([www.eurisotop.com](http://www.eurisotop.com) (24 February 2022)). Cyclohexane (CH), chloroform ( $\text{CHCl}_3$ ), ethanol (EtOH), sodium chloride (NaCl) and sodium hydrogen carbonate ( $\text{NaHCO}_3$ ) were from VWR Chemicals ([www.vwr.com](http://www.vwr.com) (24 February 2022)). 1-Bromo-4-iodobenzene, *n*-butyllithium (2.5 M in hexane) and polystyrene (PS, average M.W. 260,000 Da) were obtained from Acros Organics ([www.acros.com](http://www.acros.com) (24 February 2022)). Eudragit<sup>®</sup> RL-100 (~10% of quaternary ammonium groups, MW ~150,000) was from Degussa, Germany ([www.evonik.com](http://www.evonik.com) (24 February 2022)). Silica gel 60 (0.063–0.200 mm) and 1,2-dichloroethane were from Merck ([www.merck.at](http://www.merck.at) (24 February 2022)). Poly(ethylene terephthalate) (PET) support was received from Pütz ([www.puetz-folien.com](http://www.puetz-folien.com) (24 February 2022)). Dialysis tubing (Membra-Cel<sup>®</sup>, MWCO 7000, diameter = 16 mm) was purchased from Serva ([www.serva.de](http://www.serva.de) (24 February 2022)).

## 2.2. Measurements

$^1\text{H}$  and  $^{13}\text{C}$ -APT NMR spectra of the intermediates were recorded on a 300 MHz spectrometer and the  $^1\text{H}$  and  $^{13}\text{C}$  spectra NMR spectra of the Zn(II) Schiff base complexes on a 500 MHz instrument from Bruker ([www.bruker.com](http://www.bruker.com) (24 February 2022)) (Figures S7–S24). The residual signal of the deuterated solvent was used as an internal standard. High-resolution mass spectra of the Zn(II) Schiff bases (Figures S30–S33) were recorded on the matrix-assisted laser desorption/ionization time-of-flight mass spectrometer (MALDI-TOF MS) Micromass MALDI micro MX from Waters ([www.waters.com](http://www.waters.com) (24 February 2022)). Mass spectra for reaction monitoring and characterization of intermediates (Figures S25–S29) were acquired on an Expression CMS L compact mass spectrometer from Advion ([www.advion.com](http://www.advion.com) (24 February 2022)) with an APCI (atmospheric-pressure chemical ionization) source and quadrupole mass analyzer (range 10–2000  $m/z$ ).

Spectral properties were measured in precision cuvettes from Hellma Analytics ([www.hellma-analytics.com](http://www.hellma-analytics.com) (24 February 2022)). UV-Vis spectra were recorded on a CARY 50 UV-Vis spectrophotometer from Varian ([www.agilent.com](http://www.agilent.com) (24 February 2022)) in 10 mm cuvettes made of optical glass. Luminescence spectra were recorded on a Fluorolog-3 luminescence spectrometer ([www.horiba.com](http://www.horiba.com) (24 February 2022)) equipped with a NIR-sensitive R2658 photomultiplier from Hamamatsu. The measurements were performed in a quartz cuvette equipped with an 80 mm long tube (10 mm pass-length, Type 221). Deoxygenation of toluene solutions was performed by bubbling high-purity nitrogen (99.99999% purity) from Linde Gas ([www.linde-gas.com](http://www.linde-gas.com) (24 February 2022)) through the solution for at least 20 min. In order to record the spectra of dyes in PS, the foils were placed diagonally in a quartz glass precision cuvette (10 mm) filled with a 5 w% aqueous  $\text{Na}_2\text{SO}_3$  solution that additionally contained a catalytic amount of  $\text{CoCl}_2$ .

Luminescence decay times were measured using a spectralLED ( $\lambda = 456 \text{ nm}$ ) excitation source from Horiba on Fluorolog-3 spectrometer equipped with a DeltaHub module (Horiba). Data analysis was performed on DAS-6 Analysis software from Horiba using a mono-, bi- or tri-exponential fit. Average decay times ( $\tau$ ) of bi- and tri-exponential decays were calculated from the individual lifetimes ( $\tau_x$ ) and their amplitudes ( $B_x$ ) according to:

$$\tau = \tau_1 * B_1 + \tau_2 * B_2 + \dots \tau_z * B_z \quad (1)$$

Absolute quantum yields of prompt fluorescence ( $\Phi_{\text{prompt}}$ ) in toluene and PS were measured under aerated conditions on a Fluorolog-3 spectrometer equipped with an

integrating sphere Quanta-phi. Absolute quantum yields of delayed fluorescence ( $\Phi_{DF}$ ) were calculated according to:

$$\Phi_{DF} = \Phi_{prompt} \times \frac{A_{deoxy}}{A_{air}} - \Phi_{prompt} \quad (2)$$

where  $A_{deoxy}$  and  $A_{air}$  are the areas under the emission spectra acquired under deoxygenated and air-saturated conditions, respectively. It was assumed that due to the long decay times, the TADF emission is almost completely quenched at air-saturated conditions. Examples of the spectra under deoxygenated and air-saturated conditions measured in toluene and PS can be found in Supporting Information (Figures S1–S3).

Temperature was adjusted by using a Cary SPV—1X0 Single Cell Peltier Accessory Peltier element from Varian in combination with a F12-ED refrigerated/heating circulator from Julabo ([www.julabo.com](http://www.julabo.com) (24 February 2022)).

Temperature calibration curves were fitted via an Arrhenius type model [37]:

$$\tau = (k_0 + k_1 \times e^{-\frac{\Delta E}{k_B \times T}})^{-1} \quad (3)$$

where  $k_0$  is the temperature-independent decay rate for the excited-state deactivation,  $k_1$  is a pre-exponential factor,  $k_B$  is the Boltzmann constant,  $\Delta E$  is the energy gap between the first singlet and first triplet state, and  $T$  is the absolute temperature.

### 2.3. Preparation of Dye–Polymer Films

Dye (1 wt% in respect to the polymer) and polystyrene (10 wt% in respect to the solvent) were dissolved in chloroform to obtain a “cocktail”. The “cocktails” were knife-coated on a dust-free PET support with a wet film thickness of 25  $\mu\text{m}$  and dried for half an hour at room temperature. In case of polymer films, incorporating dye-adduct with pyridine, pyridine (100-fold excess compared to the mass of the dye) was added to the “cocktail” and the foils were dried one day in a drying chamber at 70  $^\circ\text{C}$ .

### 2.4. Fiber-Optic Setup

A sensor spot was stamped out of a dye/PS PET foil (1 wt% dye) and fixed with a metal cap on a 1 mm optical fiber. The fiber was connected to a custom version of Firesting phase fluorometer from PyroScience ([www.pyroscience.com](http://www.pyroscience.com) (24 February 2022)) that was equipped with a blue LED for the excitation. The tip of the fiber was held in a double-walled glass bottle filled with an aqueous 5 wt%  $\text{Na}_2\text{SO}_3$  solution. The temperature was adjusted by a Julabo F25-ME refrigerated/heating circulator and measured by an external PT-100 resistance thermometer.

### 2.5. Water-Dispersible Nanoparticles

A “cocktail” was prepared by dissolving dye (0.5 wt% with respect to the polymer) and RL-100 (0.2 wt% with respect to the solvent) in acetone/THF (9+1  $v/v$ ) and addition of pyridine (100-fold excess compared to the mass of the dye). Water (3 times the volume of the “cocktail”) was quickly added to the “cocktail” under vigorous stirring and the organic solvents were removed under reduced pressure. Residues of pyridine were removed by dialysis.

For temperature calibration, 2 mL of particle dispersion ( $\sim 0.4$  mg/mL) were added to 1 mL PBS puffer (10 mM, pH = 7.4) in a cuvette. The dispersion was deoxygenated by addition of 30 mg glucose monohydrate and traces of glucose oxidase.

### 2.6. Synthesis

3,6-bis(2-ethylhexyl)-9H-carbazole **1** and tetrakis(triphenylphosphine)palladium(0) ( $\text{Pd}(\text{PPh}_3)_4$ ) were synthesized according to literature procedures in [38] and [39], respectively. Flash chromatography was performed by a Biotage<sup>®</sup> Select system with additional Sfar Silica columns from Biotage ([www.biotage.com](http://www.biotage.com) (24 February 2022)).

### 2.6.1. Synthesis of 9-(4-bromophenyl)-3,6-bis(2-ethylhexyl)-9H-carbazole (2)

A Schlenk tube was loaded with compound 1 (500 mg, 1.28 mmol, 1 eq.), 1-bromo-4-iodobenzene (545 mg, 1.93 mmol, 1.5 eq.), Cs<sub>2</sub>CO<sub>3</sub> (623 mg, 1.89 mmol, 1.5 eq.) and CuI (247 mg, 1.30 mmol, 1 eq.). The tube was flushed with argon two times and DMF (3 mL) was added. The suspension was heated to 140 °C and stirred for 16 h. After full conversion, the reaction mixture was cooled to room temperature and DCM (10 mL) was added. The suspension was filtered through a glass frit and the solvent was removed under reduced pressure. The residue was purified via column chromatography (silica gel) using a gradient from CH to CH:DCM (10 + 1) as an eluent, and the product was isolated as a colorless oil (yield: 654 mg, 94%).

<sup>1</sup>H NMR (300 MHz, CD<sub>2</sub>Cl<sub>2</sub>) δ, ppm: 7.89 (s, 2H), 7.73 (d, J = 8.6 Hz, 2H), 7.48 (d, J = 8.6 Hz, 2H), 7.30 (d, J = 8.4 Hz, 2H), 7.21 (dd, J = 8.4, 1.7 Hz, 2H), 2.72 (d, J = 5.3 Hz, 4H), 1.67 (p, J = 6.2 Hz, 2H), 1.39–1.26 (m, 16H), 0.96–0.85 (m, 12H). <sup>13</sup>C NMR (76 MHz, CD<sub>2</sub>Cl<sub>2</sub>) δ, ppm: 139.74, 137.91, 134.32, 133.52, 128.94, 127.95, 124.01, 120.92, 120.70, 109.60, 42.33, 40.64, 32.95, 29.50, 26.03, 23.70, 14.51, 11.22. APCI-MS m/z: calc. for: C<sub>34</sub>H<sub>45</sub>BrN [M<sup>+</sup>]: 545.3, found: 545.4.

### 2.6.2. Synthesis of 3,6-bis(2-ethylhexyl)-9-(4-(4,4,5,5-tetramethyl-1,3,2-dioxaborolan-2-yl)phenyl)-9H-carbazole (3)

In a flame-dried and argon-flushed Schlenk tube compound 2 (451 mg, 825 μmol, 1 eq.) was dissolved in dry THF (15 mL). The solution was cooled to −78 °C and *n*-butyllithium (2.5 M in hexanes) (370 μL, 925 μmol, 1.1 eq.) was added. After stirring the mixture for 1 h at −78 °C, 2-isopropoxy-4,4,5,5-tetramethyl-1,3,2-dioxaborolane (200 μL, 981 μmol, 1.2 eq.) was added and the solution was allowed to warm to room temperature overnight. Then, water (20 mL) was added slowly, and the mixture was extracted with DCM three times. The organic phases were combined, dried over Na<sub>2</sub>SO<sub>4</sub>, and the solvent was removed under reduced pressure. The residue was purified by column chromatography (silica gel) using a gradient from CH to CH:DCM (1 + 1) as an eluent and the product was isolated as a colorless oil (yield: 340 mg, 69%).

<sup>1</sup>H NMR (300 MHz, CD<sub>2</sub>Cl<sub>2</sub>) δ, ppm: 8.00 (d, J = 8.0 Hz, 2H), 7.89 (s, 2H), 7.60 (d, J = 8.4 Hz, 2H), 7.37 (d, J = 8.4 Hz, 2H), 7.20 (dd, J = 8.4, 1.7 Hz, 2H), 2.72 (d, J = 9.1 Hz, 4H), 1.68 (q, J = 6.4 Hz, 2H), 1.38 (s, 12H), 1.37–1.25 (m, 16H), 0.96–0.84 (m, 12H). <sup>13</sup>C NMR (76 MHz, CD<sub>2</sub>Cl<sub>2</sub>) δ, ppm: 141.36, 139.67, 136.73, 134.20, 127.87, 126.17, 124.06, 120.85, 109.88, 84.61, 42.33, 40.66, 32.96, 29.51, 26.03, 25.30, 23.70, 14.51, 11.22, no signal for C(q)-boron. APCI-MS m/z: calc. for: C<sub>40</sub>H<sub>58</sub>BNO<sub>2</sub> [MH<sup>+</sup>]: 594.5, found: 594.4.

### 2.6.3. Synthesis of 4'-(3,6-bis(2-ethylhexyl)-9H-carbazol-9-yl)-3-hydroxy-[1,1'-biphenyl]-4-carbaldehyde (4)

A Schlenk tube was loaded with compound 3 (253 mg, 426 μmol, 1 eq.), 4-bromo-2-hydroxy-benzaldehyde (108 mg, 537 μmol, 1.3 eq.) and Cs<sub>2</sub>CO<sub>3</sub> (348 mg, 1.07 mmol, 2.5 eq.) under argon atmosphere and toluene (8 mL), water (4 mL) and EtOH (2 mL) were added. Then, the solution was deoxygenated with a stream of argon for 15 min and Pd(PPh<sub>3</sub>)<sub>4</sub> (15 mg, 13 μmol, 0.03 eq.) was added. The solution was heated to 90 °C and stirred overnight. After full conversion monitored via APCI-MS, the reaction mixture was allowed to cool to room temperature, saturated sodium chloride solution (10 mL) was added, and the product was extracted with DCM three times. The organic phases were combined, dried over Na<sub>2</sub>SO<sub>4</sub>, and the solvent was removed under reduced pressure. The residue was purified by flash chromatography using a gradient from CH to CH:DCM (6 + 4) as an eluent and the product was isolated as a yellow oil (yield: 232 mg, 69%).

<sup>1</sup>H NMR (300 MHz, CD<sub>2</sub>Cl<sub>2</sub>) δ, ppm: 11.17 (s, 1H), 9.96 (s, 1H), 7.95–7.84 (m, 4H), 7.71 (d, J = 8.3 Hz, 3H), 7.46–7.34 (m, 3H), 7.33 (s, 1H), 7.23 (dd, J = 8.3, 1.8 Hz, 2H), 2.73 (d, J = 5.7 Hz, 4H), 1.68 (p, J = 6.5 Hz, 2H), 1.46–1.28 (m, 16H), 0.97–0.86 (m, 12H). <sup>13</sup>C NMR (76 MHz, CD<sub>2</sub>Cl<sub>2</sub>) δ, ppm: 196.80, 162.55, 149.31, 139.74, 139.46, 138.15, 134.91, 134.34,

129.29, 127.95, 127.46, 124.11, 120.93, 120.38, 119.33, 116.09, 109.82, 42.34, 40.66, 32.96, 29.51, 26.04, 23.70, 14.52, 11.23. APCI-MS  $m/z$ : calc. for:  $C_{41}H_{51}NO_2$  [ $MH^+$ ]: 588.4, found: 588.4.

#### 2.6.4. Synthesis of 4-(3,6-bis(2-ethylhexyl)-9H-carbazol-9-yl)-2-methoxybenzaldehyde (5)

In a flame-dried and argon-flushed Schlenk tube, compound 1 (1.49 g, 3.82 mmol, 1.1 eq.), 4-bromo-2-methoxybenzaldehyde (713 mg, 3.32 mmol, 1 eq.) and  $Cs_2CO_3$  (5.51 g, 16.9 mmol, 5.0 eq.) were dissolved/suspended in dry toluene (15 mL) and the solution was deoxygenated with a stream of argon for 15 min. Afterwards, tri-tert-butylphosphonium tetrafluoroborate (80 mg, 278  $\mu$ mol, 0.08 eq) and  $Pd_2(dba)_3$  (52 mg, 56.6  $\mu$ mol, 0.02 eq.) were added, the reaction was heated to 110 °C and stirred for 21 h. After full conversion monitored via APCI-MS, the reaction was allowed to cool to room temperature and water (10 mL) was added. The product was extracted with DCM three times, dried over  $Na_2SO_4$ , and the solvent was removed under reduced pressure. The product was purified by flash chromatography using a gradient from CH to CH:DCM (1 + 1) as an eluent, and was obtained as a yellow oil (yield: 1.61 g, 83%).

$^1H$  NMR (300 MHz,  $CD_2Cl_2$ )  $\delta$ , ppm: 10.49 (s, 1H), 8.02 (d,  $J$  = 8.1 Hz, 1H), 7.89 (s, 2H), 7.47 (d,  $J$  = 8.4 Hz, 2H), 7.30 (d,  $J$  = 9.3 Hz, 2H), 7.24 (dd,  $J$  = 8.4, 1.7 Hz, 2H), 3.97 (s, 3H), 2.73 (d,  $J$  = 7.1 Hz, 4H), 1.67 (dt,  $J$  = 12.6, 6.6 Hz, 2H), 1.40–1.27 (m, 16H), 0.96–0.86 (m, 12H).  $^{13}C$  NMR (76 MHz,  $CD_2Cl_2$ )  $\delta$ , ppm: 188.89, 163.61, 145.72, 139.19, 134.94, 130.33, 128.14, 124.49, 123.66, 121.02, 118.80, 110.10, 109.96, 56.68, 42.29, 40.62, 32.94, 29.49, 26.02, 23.69, 14.50, 11.21. APCI-MS  $m/z$ : calc. for:  $C_{36}H_{48}NO_2$  [ $MH^+$ ]: 526.4, found: 526.5.

#### 2.6.5. Synthesis of 4-(3,6-bis(2-ethylhexyl)-9H-carbazol-9-yl)-2-hydroxybenzaldehyde (6)

In a flame-dried and argon-flushed Schlenk tube, compound 5 (310 mg; 590  $\mu$ mol, 1 eq.) was dissolved in dry 1,2-dichloroethane (20 mL).  $BBr_3 \cdot Me_2S$  (280 mg, 884  $\mu$ mol, 1.5 eq.) was added and the solution was stirred at 90 °C for one hour. After the mixture was cooled down to room temperature,  $H_2O$  and saturated  $NaHCO_3$  solution were added. The product was extracted with DCM three times, dried over anhydrous  $Na_2SO_4$  and the solvent was removed under reduced pressure. The product was purified by flash chromatography using a gradient from CH to CH:DCM (1 + 1) as an eluent, and was obtained as a brown oil (Yield: 284 mg, 94%).

$^1H$  NMR (300 MHz,  $CD_2Cl_2$ )  $\delta$ , ppm: 11.35 (s, 1H), 9.95 (s, 1H), 7.88 (s, 2H), 7.80 (d,  $J$  = 8.2 Hz, 1H), 7.52 (d,  $J$  = 8.4 Hz, 2H), 7.33 (dd,  $J$  = 8.2, 2.1 Hz, 1H), 7.24 (d,  $J$  = 8.2 Hz, 3H), 2.72 (d,  $J$  = 7.1 Hz, 4H), 1.71–1.63 (m, 2H), 1.32 (td,  $J$  = 13.7, 6.8 Hz, 16H), 0.90 (q,  $J$  = 7.5 Hz, 12H).  $^{13}C$  NMR (76 MHz,  $CD_2Cl_2$ )  $\delta$ , ppm: 196.13, 163.69, 146.66, 138.89, 135.82, 135.25, 128.17, 124.77, 121.01, 119.37, 117.80, 114.29, 110.38, 42.28, 40.62, 32.95, 29.49, 26.05, 23.69, 14.51, 11.22. APCI-MS  $m/z$ : calc. for:  $C_{35}H_{46}NO_2$  [ $MH^+$ ]: 512.4, found: 512.2.

#### 2.6.6. Synthesis of ZnPH-Cz

In a flame-dried and argon-flushed Schlenk tube, compound 6 (34.0 mg, 66.4  $\mu$ mol, 2.3 eq.) and 4,5-diaminophthalonitrile (4.6 mg, 29.1  $\mu$ mol, 1 eq.) were dissolved in dry EtOH (10 mL) and heated to 80 °C. After 3 h,  $Zn(AcO)_2$  (6.8 mg, 30.9  $\mu$ mol, 1.07 eq.) was added and the solution was stirred for 24 h. Water (5 mL) was added and the formed red precipitate was isolated via filtration. The crude product was purified via precipitation from DCM with EtOH/water mixture (3 + 1,  $v/v$ ) as a dark red solid (yield: 10.0 mg, 28%).

$^1H$  NMR (300 MHz,  $CD_2Cl_2$ , pyridine- $D_5$ )  $\delta$ , ppm: 8.76 (s, 2H), 7.93 (s, 2H), 7.87 (s, 4H), 7.62 (d,  $J$  = 8.2 Hz, 4H), 7.50 (d,  $J$  = 8.5 Hz, 2H), 7.23 (d,  $J$  = 8.0 Hz, 4H), 7.18 (s, 2H), 6.96 (d,  $J$  = 8.5 Hz, 2H), 2.73 (d,  $J$  = 7.1 Hz, 8H), 1.68 (p,  $J$  = 6.5 Hz, 4H), 1.40–1.29 (m, 32H), 0.91 (dt,  $J$  = 14.5, 7.0 Hz, 24H).  $^{13}C$  NMR (76 MHz,  $CD_2Cl_2$ , pyridin- $D_5$ )  $\delta$ , ppm: 176.14, 164.17, 146.79, 144.17, 138.95, 138.44, 134.82, 128.01, 124.68, 121.71, 120.86, 119.89, 118.21, 116.20, 113.42, 113.06, 111.09, 42.30, 40.66, 32.98, 30.28, 29.50, 26.09, 23.69, 14.50, 11.23. MALDI-TOF  $m/z$ : calc. for:  $C_{78}H_{91}N_6O_2Zn$  [ $MH^+$ ]: 1207.6495, found: 1207.6409.

### 2.6.7. Synthesis of ZnPH-Ph-Cz

The synthesis of **ZnPH-Ph-Cz** was performed analogously to **ZnPH-Cz**. However, 40.2 mg (68.4  $\mu\text{mol}$ , 2.1 eq) of compound **4** and 5.2 mg (32.9  $\mu\text{mol}$ , 1 eq) of 4,5-diaminophthalonitrile were used instead. They were dissolved in 4 mL dry EtOH and later 7.5 mg (34.2  $\mu\text{mol}$ , 1.04 eq) of  $\text{Zn}(\text{AcO})_2$  were added. The product was isolated as a dark red solid (yield: 30.0 mg, 67%).

$^1\text{H}$  NMR (300 MHz,  $\text{CD}_2\text{Cl}_2$ , pyridine- $D_5$ )  $\delta$ , ppm: 8.75 (s, 2H), 7.97–7.89 (m, 10H), 7.68 (d,  $J = 8.4$  Hz, 4H), 7.42 (d,  $J = 8.4$  Hz, 6H), 7.33 (s, 2H), 7.23 (dd,  $J = 8.4, 1.7$  Hz, 4H), 7.02 (dd,  $J = 8.3, 1.8$  Hz, 2H), 2.78–2.69 (m, 8H), 1.69 (p,  $J = 6.6$  Hz, 4H), 1.42–1.28 (m, 32H), 0.92 (dt,  $J = 14.1, 7.0$  Hz, 24H).  $^{13}\text{C}$  NMR (76 MHz,  $\text{CD}_2\text{Cl}_2$ , pyridine- $D_5$ )  $\delta$ , ppm: 175.45, 164.68, 148.54, 144.22, 139.78, 138.99, 138.89, 137.62, 134.25, 129.03, 127.93, 127.25, 124.08, 122.64, 121.78, 120.89, 118.98, 116.23, 114.65, 113.08, 109.92, 42.35, 40.70, 32.99, 29.52, 26.07, 23.70, 14.51, 11.23. MALDI-TOF  $m/z$ : calc. for:  $\text{C}_{90}\text{H}_{99}\text{N}_6\text{O}_2\text{Zn}$  [ $\text{MH}^+$ ]: 1359.7120, found: 1359.7860.

### 2.6.8. Synthesis of ZnPZ-Cz

The synthesis of **ZnPZ-Cz** was performed analogously to **ZnPH-Cz**. However, 42.7 mg (83.4  $\mu\text{mol}$ , 2.1 eq) of compound **6** and 6.3 mg (39.3  $\mu\text{mol}$ , 1 eq) of 5,6-diamino-2,3-pyrazinedicarbonitrile dissolved in 10 mL dry EtOH were used instead. Later, 9.7 mg (44.2  $\mu\text{mol}$ , 1.1 eq) of  $\text{Zn}(\text{AcO})_2$  were added. The product was isolated as a dark red solid (yield: 10.1 mg, 21%).

$^1\text{H}$  NMR (300 MHz,  $\text{CD}_2\text{Cl}_2$ , pyridine- $D_5$ )  $\delta$ , ppm: 9.35 (s, 2H), 7.86 (s, 4H), 7.65 (d,  $J = 8.5$  Hz, 4H), 7.56 (d,  $J = 8.7$  Hz, 2H), 7.28–7.17 (m, 6H), 7.03 (d,  $J = 8.5$  Hz, 2H), 2.73 (d,  $J = 7.0$  Hz, 8H), 1.68 (p,  $J = 7.0$  Hz, 4H), 1.37–1.27 (m, 32H), 0.90 (dt,  $J = 17.6, 6.9$  Hz, 24H).  $^{13}\text{C}$  NMR (76 MHz,  $\text{CD}_2\text{Cl}_2$ , pyridine- $D_5$ )  $\delta$ , ppm: 178.97, 165.98, 149.44, 148.63, 139.58, 138.92, 138.63, 135.35, 128.18, 127.25, 125.00, 122.47, 120.94, 118.94, 114.62, 111.43, 42.28, 40.67, 32.97, 29.50, 26.09, 23.69, 14.50, 11.24. MALDI-TOF  $m/z$ : calc. for:  $\text{C}_{76}\text{H}_{89}\text{N}_8\text{O}_2\text{Zn}$  [ $\text{MH}^+$ ]: 1209.6400, found: 1209.7391.

### 2.6.9. Synthesis of ZnPZ-Ph-Cz

The synthesis of **ZnPZ-Ph-Cz** was performed analogously to **ZnPH-Cz**. However, 31.2 mg (53.1  $\mu\text{mol}$ , 2.3 eq) of compound **4** and 3.7 mg (23.1  $\mu\text{mol}$ , 1 eq) of 5,6-diamino-2,3-pyrazinedicarbonitrile dissolved in 5 mL dry EtOH were used instead. Later 5.3 mg (24.3  $\mu\text{mol}$ , 1.05 eq) of  $\text{Zn}(\text{AcO})_2$  were added. The product was isolated as a dark red solid (yield: 10.4 mg, 33%).

$^1\text{H}$  NMR (300 MHz,  $\text{CD}_2\text{Cl}_2$ , pyridine- $D_5$ )  $\delta$ , ppm: 9.38 (s, 2H), 7.96 (d,  $J = 8.0$  Hz, 4H), 7.90 (s, 4H), 7.71 (d,  $J = 8.4$  Hz, 4H), 7.47 (d,  $J = 8.9$  Hz, 2H), 7.43 (d,  $J = 8.2$  Hz, 4H), 7.34 (s, 2H), 7.23 (d,  $J = 7.3$  Hz, 4H), 7.07 (d,  $J = 8.5$  Hz, 2H), 2.78–2.69 (m, 8H), 1.71–1.65 (m, 4H), 1.40–1.29 (m, 34H), 0.92 (dt,  $J = 14.1, 7.0$  Hz, 24H).  $^{13}\text{C}$  NMR (76 MHz,  $\text{CD}_2\text{Cl}_2$ , pyridine- $D_5$ )  $\delta$ , ppm: 178.47, 162.98, 150.44, 139.70, 139.52, 138.62, 138.28, 138.03, 134.36, 129.15, 127.97, 127.49, 127.28, 126.95, 124.14, 120.92, 119.76, 116.07, 114.64, 109.92, 42.35, 40.70, 32.99, 29.52, 26.07, 23.71, 14.51, 11.24. MALDI-TOF  $m/z$ : calc. for:  $\text{C}_{88}\text{H}_{97}\text{N}_8\text{O}_2\text{Zn}$  [ $\text{MH}^+$ ]: 1361.7026, found: 1361.7240.

## 3. Results and Discussion

### 3.1. Synthesis

The Zn(II) Schiff base complexes consist of a carbazole donor moiety and either a 2,3-pyrazinedicarbonitrile or a phthalonitrile acceptor moiety. The carbazole units bear two 2-ethylhexyl chains which significantly increase the solubility of the complexes compared to the previously reported *t*-butyl substituted derivative [36]. The alkyl-substituted carbazole **1** is conveniently prepared in two steps from commercially available 9H-carbazole following a literature method [38]. Starting from compound **1**, the carbazole-substituted hydroxybenzaldehyde precursor **6** and its phenyl extended analogue **4** are synthesized in two and four steps, respectively (Figure 2a). In a last step, the Zn(II) Schiff base complexes

are formed in a one-pot procedure [40–42] from the corresponding diamine, zinc acetate dihydrate and the precursors **4** or **6** (Figure 2b).

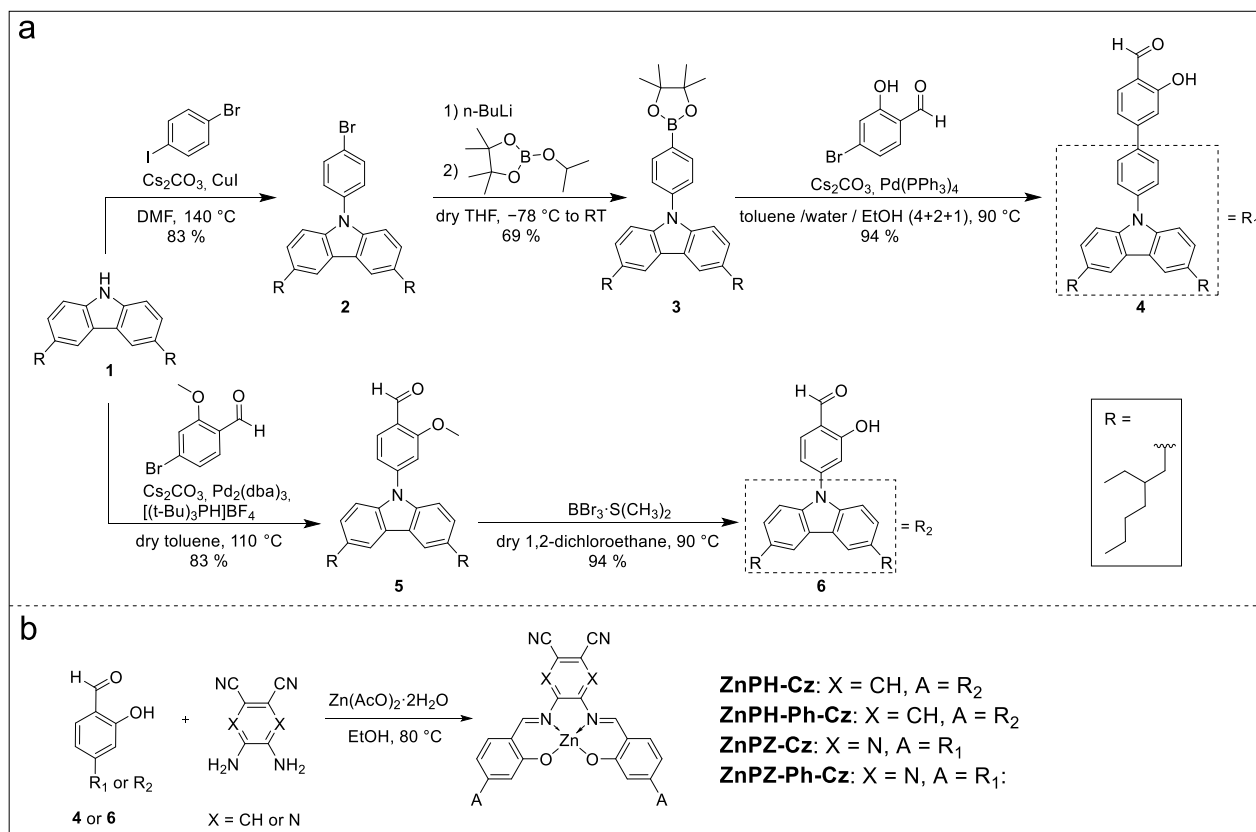


**Figure 2.** Synthesis of the dye precursors (a) and the Zn(II) Schiff base complexes (b).

### 3.2. Photophysical Properties

Figure 3 shows absorption and emission spectra of the four complexes in toluene. The complexes bearing the phthalonitrile acceptor (**ZnPH-Cz** and **ZnPH-Ph-Cz**) absorb in the blue part and emit in the green–yellow of the electromagnetic spectrum (Figure 3a). The absorption and emission spectra of **ZnPH-Cz** are almost identical to those of **Zn-2** [36], which bears *tert*-butyl groups instead of 2-ethylhexyl substituents (Table 1). A pronounced bathochromic shift of absorption and emission spectra is observed upon substitution of phthalonitrile with 2,3-pyrazinedicarbonitrile (Figure 3b), which is a significantly stronger electron acceptor than phthalonitrile [43]. These dyes (**ZnPZ-Cz** and **ZnPZ-Ph-Cz**) show the absorption maxima in the green part of the spectrum and emit red light. The molar absorption coefficients are slightly higher for the dyes with 2,3-pyrazinedicarbonitrile acceptor compared to the corresponding compounds based on phthalonitrile (Table 1). Introduction of phenyl spacer decreases molar absorption coefficients by ~30%. Notably, in both systems, the UV absorption of the dyes with linker is strongly enhanced.

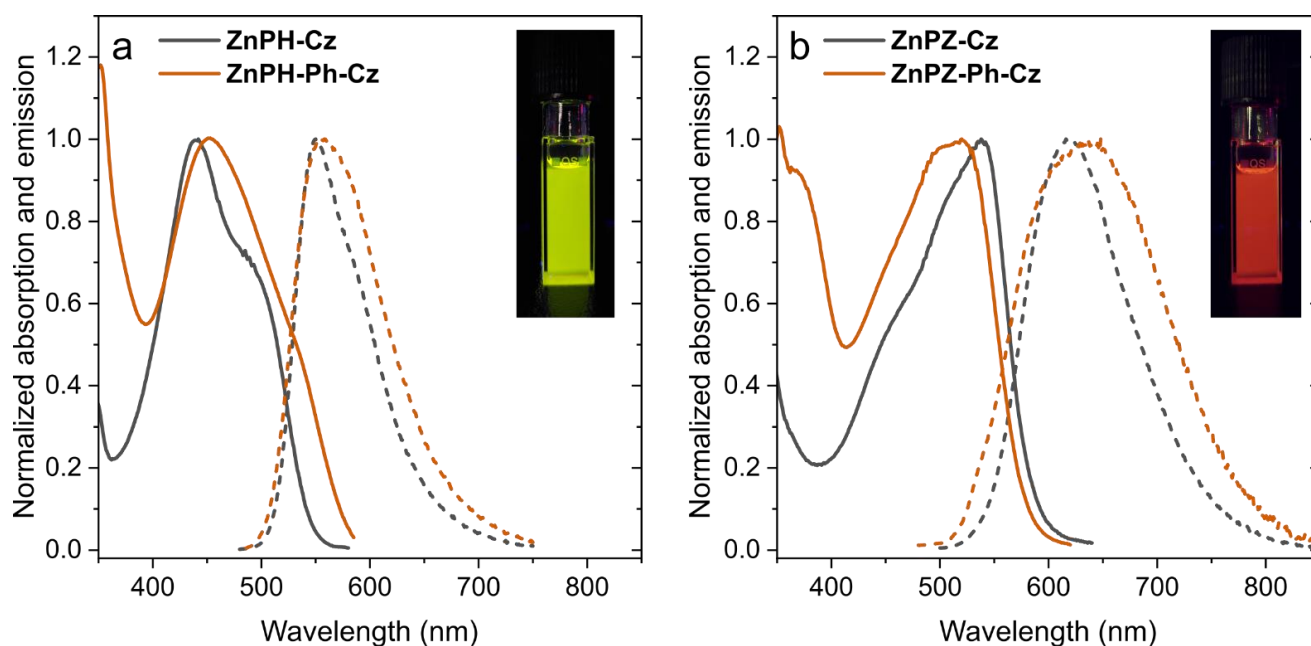


**Figure 3.** Absorption (solid lines) and emission (dashed lines) spectra of Zn(II) Schiff base complexes with phthalonitrile (a) and 2,3-pyrazinedicarbonitrile (b) as acceptor moiety acquired in (anoxic) toluene at 25 °C. The insets show photographic images of anoxic toluene solutions of **ZnPH-Cz** (a) and **ZnPZ-Cz** (b) under 366 nm UV-excitation.

**Table 1.** Photophysical properties of Zn(II) Schiff base complexes in toluene at 25 °C.

Dye	$\lambda_{\max, \text{abs}}$ (nm)	$\epsilon$ ( $\text{M}^{-1} \text{cm}^{-1}$ )	$\lambda_{\max, \text{em}}$ (nm) <sup>c</sup>	$\tau_{\text{TADF}}$ ( $\mu\text{s}$ ) <sup>c</sup>	$\Phi_{\text{PF}}$ (%)	$\Phi_{\text{TADF}}$ (%) <sup>c</sup>
Zn-2 <sup>a</sup>	435, 490 <sup>b</sup>	$39,000 \pm 600$	547	$435 \pm 1$	$27 \pm 2$	$14 \pm 2$
ZnPH-Cz	442, 490 <sup>b</sup>	$37,200 \pm 200$	550	$945 \pm 6$	$18.7 \pm 0.6$	$18.3 \pm 0.8$
ZnPH-Ph-Cz	455, 530 <sup>b</sup>	$25,300 \pm 300$	558	$1040 \pm 5$	$14.0 \pm 0.2$	$15.4 \pm 0.4$
ZnPZ-Cz	538	$44,200 \pm 100$	616	$144 \pm 1$	$9.1 \pm 0.8$	$4.0 \pm 0.4$
ZnPZ-Ph-Cz	520	$32,500 \pm 100$	648	$236 \pm 3$	$1.6 \pm 0.1$	$0.3 \pm 0.1$

<sup>a</sup> Ref. [36]; <sup>b</sup> shoulder; <sup>c</sup> anoxic conditions.

The emission spectra of the dyes with 2,3-pyrazinedicarbonitrile acceptor (**ZnPZ-Cz** and **ZnPZ-Ph-Cz**) are significantly broader (FWHM of  $2860$  and  $3870 \text{ cm}^{-1}$ , respectively) than for the corresponding dyes bearing phthalonitrile acceptor (FWHM of  $2380$  and  $2830 \text{ cm}^{-1}$  for **ZnPH-Cz** and **ZnPH-Ph-Cz**, respectively). It is also evident that the dyes with phenyl linker show slightly broader emission spectra. This effect can be explained by more restricted rotation between the donor and acceptor units in case of the dyes bearing no spacer which favors sharper emission bands [43]. Unfortunately, substitution of phthalonitrile with 2,3-pyrazinedicarbonitrile also results in significant decrease of the luminescence quantum yields, both for prompt fluorescence and TADF (Table 1). The effect is milder in case of the phthalonitrile acceptor (**ZnPH-Ph-Cz**), but is much more pronounced for the dye bearing 2,3-pyrazinedicarbonitrile **ZnPZ-Ph-Cz** that shows poor prompt and delayed fluorescence in solution (Table 1).

The TADF decay times, measured in anoxic toluene, vary between  $144 \mu\text{s}$  and  $1040 \mu\text{s}$  (Table 1) and are non-monoexponential, with the exception of **ZnPH-Cz** (Figure S4). The shortest decay times were obtained for **ZnPZ-Cz** and **ZnPZ-Ph-Cz**, which bear the stronger 2,3-pyrazinedicarbonitrile acceptor (Table 1). As can be seen, the TADF decay times are increased upon introduction of phenyl linker. The observed effects may be explained by an increased energy gap between first singlet and triplet state ( $\Delta E_{\text{ST}}$ ) upon introduction of the linker [43]. Particularly, the energy of the singlet state is increased due to less efficient separation between HOMO (usually located on the donor unit) and LUMO (usually located

on the acceptor unit), and the triplet state is reduced in energy by conjugation extending effects [43].

### 3.3. Properties of Immobilized Dyes

Polystyrene was used as a model matrix for evaluation of the photophysical properties of the new dyes in a rigid environment since immobilization of dyes is essential for many applications, varying from sensors to OLEDs. Photophysical properties of the immobilized emitters are summarized in Table 2. All four emitter-polymer materials were characterized as with and without additional pyridine. The pyridine coordinates on the free axial positions of the zinc metal center and is supposed to prevent the emitters from aggregation.

**Table 2.** Photophysical properties of Zn(II) Schiff base complexes with and without pyridine in rigid polystyrene matrix at 25 °C.

Dye	$\lambda_{\max, \text{abs}}$ (nm)	$\lambda_{\max, \text{em}}$ (nm)	$\tau_{\text{TADF}}$ ( $\mu\text{s}$ ) <sup>b</sup>	$\Phi_{\text{PF}}$ (%)	$\Phi_{\text{TADF}}$ (%) <sup>b</sup>	$d\tau/dT$ (%/K) <sup>b</sup>
Zn-2 <sup>a</sup>	446	547	1450 ± 10	18 ± 2	47 ± 6	−3.5
ZnPH-Cz	439	554	1240 ± 40	15.9 ± 0.2	15.8 ± 0.2	−3.4
ZnPH-Cz/Py	449	552	1150 ± 10	21.1 ± 0.3	46.8 ± 0.4	−3.6
ZnPH-Ph-Cz	448	555	3530 ± 10	4.4 ± 0.1	6.5 ± 0.2	−3.3
ZnPH-Ph-Cz/Py	444	561	1930 ± 30	10.9 ± 0.2	33.3 ± 0.4	−3.6
ZnPZ-Cz	522	626	132 ± 4	5.6 ± 0.1	1.5 ± 0.1	−3.3
ZnPZ-Cz/Py	544	602	328 ± 3	6.8 ± 0.4	5.6 ± 0.4	−3.7
ZnPZ-Ph-Cz	510	611	991 ± 2	1.6 ± 0.1	0.7 ± 0.1	−3.4
ZnPZ-Ph-Cz/Py	510	594	1302 ± 7	8.1 ± 0.6	7.9 ± 0.6	−3.2

<sup>a</sup> Ref. [36]; <sup>b</sup> anoxic conditions.

Immobilization only slightly affects the absorption and emission spectra. However, both the TADF decay times and the quantum yields are strongly affected by immobilization. The TADF decays of all four complexes (with and without pyridine) are non-monoexponential (Figure S4). For immobilized ZnPH-Cz and ZnPZ-Cz, the decay times are comparable to those obtained in toluene solution. On the other hand, the dyes with phenyl spacer (ZnPH-Ph-Cz and ZnPZ-Ph-Cz) show 3–4-fold increase of the decay times upon immobilization. This is a drawback with respect to potential applications as molecular thermometers since the longer decay times favor higher cross-sensitivity of the materials to molecular oxygen. Interestingly, coordination of pyridine results in decrease of TADF decay times in case of phthalonitrile-based emitters ZnPH-Cz/Py and ZnPH-Ph-Cz/Py, whereas the opposite effect is observed for the 2,3-pyrazinedicarbonitrile-based emitters ZnPZ-Cz/Py and ZnPZ-Ph-Cz/Py.

Without additional pyridine, only ZnPH-Cz shows acceptable quantum yields of the delayed fluorescence, whereas for other dyes, TADF efficiency is moderate to poor. In contrast, all emitters with coordinated pyridine show an increase in both prompt and TADF quantum yields (up to 47% for ZnPH-Cz/Py). For ZnPH-Cz/Py and ZnPH-Ph-Cz/Py the TADF is by far more efficient than prompt fluorescence emission. The pyridine-coordinated emitter ZnPH-Cz/Py, apart from good solubility, shows excellent photophysical properties in rigid matrix that makes it the most promising candidate for practical applications.

Figure 4 exemplifies the effect of temperature of the TADF decay time for ZnPH-Cz and ZnPH-Cz/Py in polystyrene matrix. The dependencies for the other complexes can be found in Supporting Information (Figures S5 and S6). Evidently, the TADF decay times strongly decrease with temperature which is the prerequisite for the application of the emitters as molecular thermometers with self-referenced decay time read-out. Interestingly, structural modifications have almost no effect on the temperature sensitivity. In fact, the temperature coefficients for all the dyes including previously reported Zn-2 vary in a very narrow range (from −3.2 to −3.7%/K at 25 °C, Table 2). Such temperature coefficients are very high and exceed those for most of the reported molecular thermometers and thermographic phosphors [36].

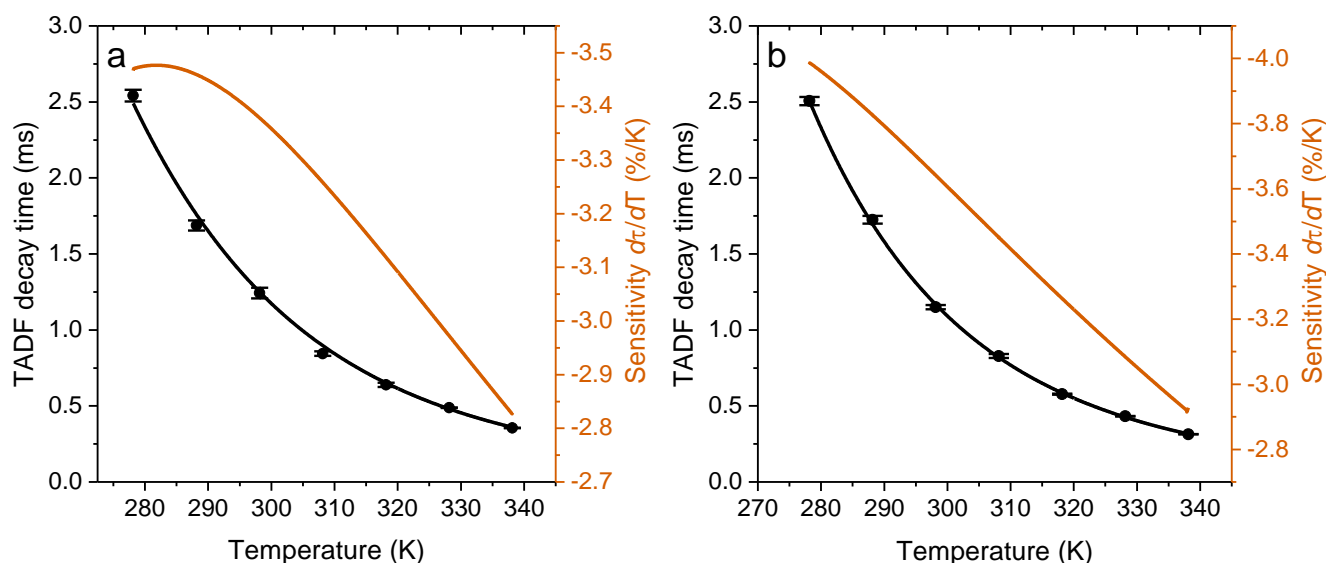


**Figure 4.** Temperature dependency of TADF decay times for ZnPH-Cz (a) and for ZnPH-Cz/Py (b) immobilized in PS matrix acquired in deoxygenized solution. In each temperature calibration cycle, three decay time measurements were made at each temperature. The calibration cycle was repeated three times.

### 3.4. Polymer-Based Sensor Materials

In order to evaluate potential applicability of the dyes, the most promising candidate **ZnPH-Cz/Py** was evaluated in two different sensor formats: a fiber-optic sensor and nanoparticles. In the first format, the dye was embedded in a polystyrene layer coated on a transparent polyethylene terephthalate support. The sensor foil was fixed on the tip of an optical fiber and readout was performed with a custom version (excitation with a blue LED excitation source) of a commercially available phase fluorometer (Firesting, PyroScience). Figure 5 shows the measured phase shift of three temperature cycles between 20 °C and 50 °C acquired in anoxic solutions. The sensor shows reproducible performance and good resolution, but also demonstrates an important limitation of the frequency-domain read-out: due to significant contribution of prompt fluorescence (~30%, Table 2), the measured phase angle is significantly lower than, e.g., for phosphorescent dyes with the same excited state decay time. Clearly, the most serious limitation of the sensor is that it operates in the anoxic environment but different approaches (e.g., using oxygen scavengers [36]) may be feasible to overcome this problem.

Nanoparticles for potential application in intracellular measurements have also been prepared. **ZnPH-Cz/Py** was embedded in commercially available Eudragit RL-100 polymer. RL-100 nanoparticles bear positively charged quaternary ammonium groups on their surface, have an average size of ~30 nm, and efficiently stain a variety of cells that enable intracellular measurements [44]. They are usually prepared by a common precipitation technique [45]. In short, the dye and the polymer are dissolved in a water miscible organic solvent (usually acetone), followed by addition of water under vigorous stirring and removal of the organic solvent under reduced pressure.

For characterization, the oxygen from the aqueous particle dispersion was removed by glucose and glucose oxidase. PBS buffer was added to avoid potential degradation of **ZnPH-Cz/Py** in acidic environment that would otherwise be generated by formation of gluconic acid during the enzymatic reaction. Anoxic puffer systems that are known from super-resolution microscopy [46] can be used if the material is further applied for intracellular temperature measurements.

Excitation and emission spectra (Figure 6a) indicate a slight hypsochromic shift compared to polystyrene. Remarkably, the TADF decay times in the nanoparticles increase by about 2-fold (25 °C) compared to polystyrene (Figure 6b). Favorably for optical temperature

measurement, the temperature sensitivity is also further enhanced to  $-5.4\%/K$  at  $25\text{ }^{\circ}\text{C}$ . A possible explanation for the longer TADF decay times and higher sensitivity could be the more hydrophilic environment which affects the donor and acceptor orientation, as well as the charge distribution of the dye. This effect may be further explored in future to prepare more sensitive bulk optodes and fiber-optic sensors on the basis of the nanoparticles.

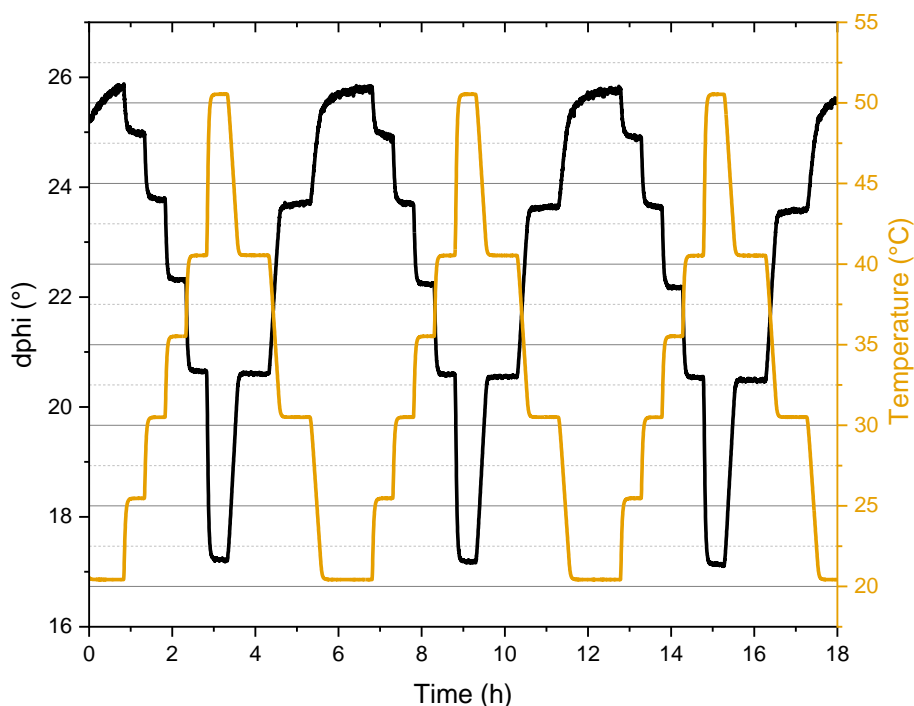


**Figure 5.** Luminescence signal of ZnPH-Cz/Py in polystyrene (modulation frequency 200 Hz) under anoxic conditions (aqueous solution with 5 w%  $\text{Na}_2\text{SO}_3$ ). The temperature was measured by a PT-100 resistance thermometer.

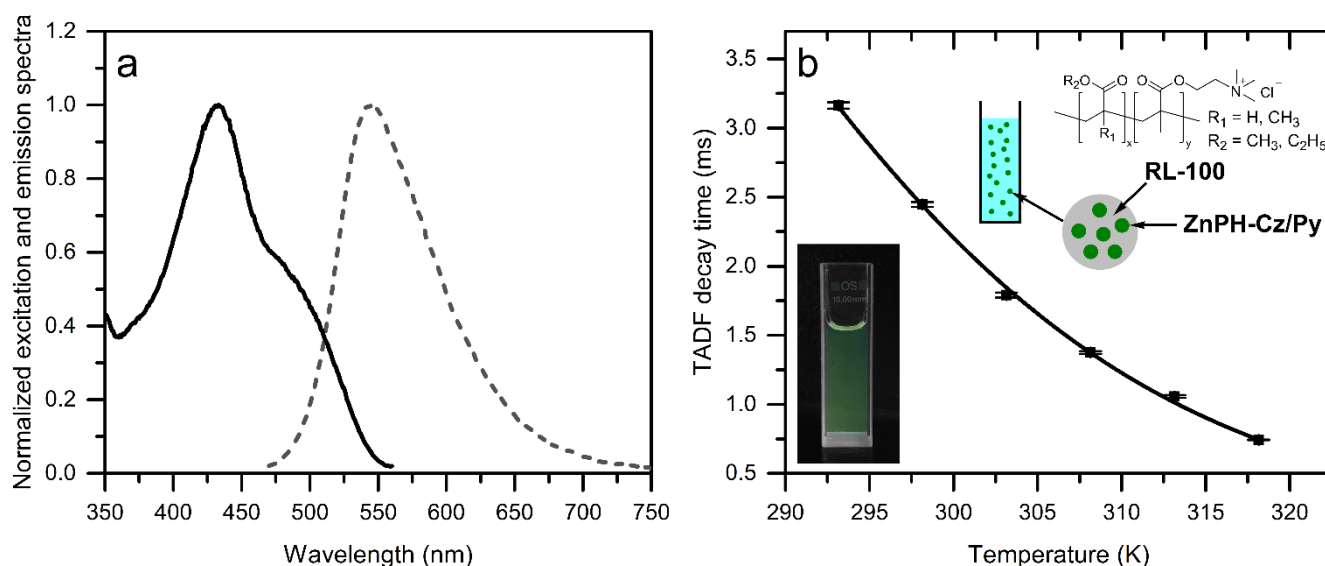


**Figure 6.** Excitation (solid lines) and emission (dashed lines) spectra (a) and temperature dependency of TADF decay times (b) for ZnPH-Cz/Py immobilized in RL-100 nanoparticles acquired under anoxic conditions. For the temperature dependency measurements, two calibration cycles were performed. In each cycle, three decay time measurements were made at each temperature. The inset shows a photographic image of the particle dispersion ( $0.4\text{ mg/mL}$ ) under UV irradiation.

#### 4. Conclusions

In conclusion, four new Zn(II) Schiff base complexes combining a carbazole based electron donor and two different electron acceptors and optionally an additional phenyl linker were prepared. The absorption and emission spectra show significant bathochromic shift upon substitution of phthalonitrile by stronger electron accepting 2,3-pyrazinedicarbonitrile unit which is accompanied by decrease of TADF decay times by several fold. Unfortunately, the dyes utilizing 2,3-pyrazinedicarbonitrile also show strongly reduced TADF quantum yield. Introduction of a phenyl linker negatively affects the quantum yields and leads to the increase of the TADF lifetimes which is undesirable in view of oxygen crosstalk for temperature sensing applications. The addition of pyridine significantly improves TADF quantum yields of all four emitters immobilized in a polymer matrix. Among the dyes investigated, the pyridine coordinated emitter bearing phthalonitrile acceptor and no linker (**ZnPH-Cz/Py**) is found to be the most promising for optical temperature sensing applications. It combines acceptably good solubility in organic solvents and polymers due to four bulky 2-ethylhexyl units, excellent photophysical properties and very high temperature coefficients of the TADF decay times at ambient conditions. The temperature sensitivity is enhanced even further if the dye is embedded into RL-100 nanoparticles that due to excellent cell-staining capabilities may represent an interesting tool for intracellular imaging of temperature distribution.

**Supplementary Materials:** The following are available online at <https://www.mdpi.com/article/10.3390/chemosensors10030091/s1>, Figure S1: Emission spectra of **ZnPH-Cz** (a), **ZnPH-Ph-Cz** (b), **ZnPZ-Cz** (c) and **ZnPZ-Ph-Cz** (d) measured in toluene under anoxic (degassed with high purity nitrogen) and air-saturated conditions, Figure S2: Emission spectra of **ZnPH-Cz** (a), **ZnPH-Ph-Cz** (b), **ZnPZ-Cz** (c) and **ZnPZ-Ph-Cz** (d) measured in toluene under anoxic conditions (aqueous solution with 5 w% Na<sub>2</sub>SO<sub>3</sub> and traces of CoCl<sub>2</sub>) and air-saturated conditions, **Figure S3:** Emission spectra of **ZnPH-Cz** (a), **ZnPH-Ph-Cz** (b), **ZnPZ-Cz** (c) and **ZnPZ-Ph-Cz** (d) with pyridine as axial ligands measured in polystyrene under anoxic conditions (aqueous solution with 5 w% Na<sub>2</sub>SO<sub>3</sub> and traces of CoCl<sub>2</sub>) and air-saturated conditions, Figure S4: TADF decay of **ZnPH-Cz** (a), **ZnPH-Ph-Cz** (b), **ZnPZ-Cz** (c) and **ZnPZ-Ph-Cz** (d) in toluene and polystyrene (with and without pyridine) under anoxic conditions at 25 °C, Figure S5: Temperature dependency of TADF lifetimes between 5 and 65 °C for **ZnPZ-Cz** (a), **ZnPZ-Ph-Cz** (b) and **ZnPH-Ph-Cz** (c) in PS matrix under anoxic conditions (aqueous solution with 5 w% Na<sub>2</sub>SO<sub>3</sub> and traces of CoCl<sub>2</sub>). In each temperature calibration cycle, three decay time measurements were made at each temperature. The calibration cycle was repeated three times, Figure S6: Temperature dependency of TADF lifetimes between 5 and 65 °C for **ZnPZ-Cz** (a), **ZnPZ-Ph-Cz** (b) and **ZnPH-Ph-Cz** (c) with pyridine in PS matrix under anoxic conditions (aqueous solution with 5 w% Na<sub>2</sub>SO<sub>3</sub> and traces of CoCl<sub>2</sub>). In each temperature calibration cycle, three decay time measurements were made at each temperature. The calibration cycle was repeated three times, Figure S7: <sup>1</sup>H NMR (300 MHz, CD<sub>2</sub>Cl<sub>2</sub>) of **2**, Figure S8: <sup>13</sup>C-APT NMR (76 MHz, CD<sub>2</sub>Cl<sub>2</sub>) of **2**, Figure S9: <sup>1</sup>H NMR (300 MHz, CD<sub>2</sub>Cl<sub>2</sub>) of **3**, Figure S10: <sup>13</sup>C-APT NMR (76 MHz, CD<sub>2</sub>Cl<sub>2</sub>) of **3**, Figure S11: <sup>1</sup>H NMR (300 MHz, CD<sub>2</sub>Cl<sub>2</sub>) of **4**, Figure S12: <sup>13</sup>C-APT NMR (76 MHz, CD<sub>2</sub>Cl<sub>2</sub>) of **4**, Figure S13: <sup>1</sup>H NMR (300 MHz, CD<sub>2</sub>Cl<sub>2</sub>) of **5**, Figure S14: <sup>13</sup>C-APT NMR (76 MHz, CD<sub>2</sub>Cl<sub>2</sub>) of **5**, Figure S15: <sup>1</sup>H NMR (300 MHz, CD<sub>2</sub>Cl<sub>2</sub>) of **6**, Figure S16: <sup>13</sup>C-APT NMR (76 MHz, CD<sub>2</sub>Cl<sub>2</sub>) of **6**, Figure S17: <sup>1</sup>H NMR (500 MHz, CD<sub>2</sub>Cl<sub>2</sub>, pyridine-D<sub>5</sub>) of **ZnPH-Cz**, Figure S18: <sup>13</sup>C-NMR (126 MHz, CD<sub>2</sub>Cl<sub>2</sub>, pyridine-D<sub>5</sub>) of **ZnPH-Cz**, Figure S19: <sup>1</sup>H NMR (500 MHz, CD<sub>2</sub>Cl<sub>2</sub>, pyridine-D<sub>5</sub>) of **ZnPH-Ph-Cz**, Figure S20: <sup>13</sup>C-NMR (126 MHz, CD<sub>2</sub>Cl<sub>2</sub>, pyridine-D<sub>5</sub>) of **ZnPH-Ph-Cz**, Figure S21: <sup>1</sup>H NMR (500 MHz, CD<sub>2</sub>Cl<sub>2</sub>, pyridine-D<sub>5</sub>) of **ZnPZ-Cz**, Figure S22: <sup>13</sup>C-NMR (126 MHz, CD<sub>2</sub>Cl<sub>2</sub>, pyridine-D<sub>5</sub>) of **ZnPZ-Cz**, Figure S23: <sup>1</sup>H NMR (500 MHz, CD<sub>2</sub>Cl<sub>2</sub>, pyridine-D<sub>5</sub>) of **ZnPZ-Ph-Cz**, Figure S24: <sup>13</sup>C-NMR (126 MHz, CD<sub>2</sub>Cl<sub>2</sub>, pyridine-D<sub>5</sub>) of **ZnPZ-Ph-Cz**, Figure S25: Mass spectra (APCI-MS) of **2**, Figure S26: Mass spectra (APCI-MS) of **3**, Figure S27: Mass spectra (APCI-MS) of **4**, Figure S28: Mass spectra (APCI-MS) of **5**, Figure S29: Mass spectra (APCI-MS) of **6**, Figure S30: Mass spectra (MALDI-TOF) of **ZnPH-Cz** in dithranol matrix, Figure S31: Mass spectra (MALDI-TOF) of **ZnPH-Ph-Cz** in dithranol matrix, Figure S32: Mass spectra (MALDI-TOF) of **ZnPZ-Cz** in dithranol matrix, Figure S33: Mass spectra (MALDI-TOF) of **ZnPZ-Ph-Cz** in dithranol matrix.

**Author Contributions:** A.R. performed the experiments and prepared initial draft of the manuscript. L.E. performed synthesis and characterization of some of the compounds. A.S. and S.M.B. conceived and directed the study. All authors contributed to the analysis of the results and to the writing of the manuscript. All authors have read and agreed to the published version of the manuscript.

**Funding:** This research was funded by Austrian Science Fund FWF, grant number P32079-N37.

**Institutional Review Board Statement:** Not applicable.

**Informed Consent Statement:** Not applicable.

**Data Availability Statement:** Not applicable.

**Conflicts of Interest:** The authors declare no conflict of interest.

## References

1. Wang, X.D.; Wolfbeis, O.S.; Meier, R.J. Luminescent probes and sensors for temperature. *Chem. Soc. Rev.* **2013**, *42*, 7834–7869. [[CrossRef](#)] [[PubMed](#)]
2. Ogle, M.M.; Smith McWilliams, A.D.; Jiang, B.; Martí, A.A. Latest Trends in Temperature Sensing by Molecular Probes. *ChemPhotoChem* **2020**, *4*, 255–270. [[CrossRef](#)]
3. Jaque, D.; Vetrone, F. Luminescence nanothermometry. *Nanoscale* **2012**, *4*, 4301–4326. [[CrossRef](#)] [[PubMed](#)]
4. Dramićanin, M. *Luminescence Thermometry: Methods, Materials, and Applications*; Woodhead Publishing: Sawston, UK, 2018; ISBN 9780081020296.
5. Bai, T.; Gu, N. Micro/nanoscale thermometry for cellular thermal sensing. *Small* **2016**, *12*, 4590–4610. [[CrossRef](#)]
6. Jenkins, J.; Borisov, S.M.; Papkovsky, D.B.; Dmitriev, R.I. Sulforhodamine Nanothermometer for Multiparametric Fluorescence Lifetime Imaging Microscopy. *Anal. Chem.* **2016**, *88*, 10566–10572. [[CrossRef](#)] [[PubMed](#)]
7. Wu, Y.; Liu, J.; Ma, J.; Liu, Y.; Wang, Y.; Wu, D. Ratiometric Nanothermometer Based on Rhodamine Dye-Incorporated F127-Melamine-Formaldehyde Polymer Nanoparticle: Preparation, Characterization, Wide-Range Temperature Sensing, and Precise Intracellular Thermometry. *ACS Appl. Mater. Interfaces* **2016**, *8*, 14396–14405. [[CrossRef](#)]
8. Wang, H.; Wu, Y.; Tao, P.; Fan, X.; Kuang, G.C. BODIPY-Based Oligo (ethylene glycol) Dendrons as Fluorescence Thermometers: When Thermoresponsiveness Meets Intramolecular Electron/Charge Transfer. *Chem. A Eur. J.* **2014**, *20*, 16634–16643. [[CrossRef](#)]
9. Ogle, M.M.; Smith McWilliams, A.D.; Ware, M.J.; Curley, S.A.; Corr, S.J.; Martí, A.A. Sensing Temperature in Vitro and in Cells Using a BODIPY Molecular Probe. *J. Phys. Chem. B* **2019**, *123*, 7282–7289. [[CrossRef](#)]
10. Carlotti, M.; Gullo, G.; Battisti, A.; Martini, F.; Borsacchi, S.; Geppi, M.; Ruggeri, G.; Pucci, A. Thermochromic polyethylene films doped with perylene chromophores: Experimental evidence and methods for characterization of their phase behaviour. *Polym. Chem.* **2015**, *6*, 4003–4012. [[CrossRef](#)]
11. Chandrasekharan, N.; Kelly, L.A. A dual fluorescence temperature sensor based on perylene/excimer interconversion. *J. Am. Chem. Soc.* **2001**, *123*, 9898–9899. [[CrossRef](#)]
12. Bustamante, N.; Ielasi, G.; Bedoya, M.; Orellana, G. Optimization of temperature sensing with polymer-embedded luminescent Ru(II) complexes. *Polymers* **2018**, *10*, 234. [[CrossRef](#)]
13. Fischer, L.H.; Stich, M.I.J.; Wolfbeis, O.S.; Tian, N.; Holder, E.; Schäferling, M. Red- and Green-Emitting Iridium(III) Complexes for a Dual Barometric and Temperature-Sensitive Paint. *Chem. A Eur. J.* **2009**, *15*, 10857–10863. [[CrossRef](#)] [[PubMed](#)]
14. Borisov, S.M.; Wolfbeis, O.S. Temperature-sensitive europium(III) probes and their use for simultaneous luminescent sensing of temperature and oxygen. *Anal. Chem.* **2006**, *78*, 5094–5101. [[CrossRef](#)] [[PubMed](#)]
15. Khalil, G.E.; Lau, K.; Phelan, G.D.; Carlson, B.; Gouterman, M.; Callis, J.B.; Dalton, L.R. Europium beta-diketonate temperature sensors: Effects of ligands, matrix, and concentration. *Rev. Sci. Instrum.* **2004**, *75*, 192–206. [[CrossRef](#)]
16. Karakus, C.; Fischer, L.H.; Schmeding, S.; Hummel, J.; Risch, N.; Schäferling, M.; Holder, E. Oxygen and temperature sensitivity of blue to green to yellow light-emitting Pt(II) complexes. *Dalt. Trans.* **2012**, *41*, 9623–9632. [[CrossRef](#)] [[PubMed](#)]
17. Borisov, S.M.; Pommer, R.; Svec, J.; Peters, S.; Novakova, V.; Klimant, I. New red-emitting Schiff base chelates: Promising dyes for sensing and imaging of temperature and oxygen via phosphorescence decay time. *J. Mater. Chem. C* **2018**, *6*, 8999–9009. [[CrossRef](#)] [[PubMed](#)]
18. Uchiyama, S.; Gota, C.; Tsuji, T.; Inada, N. Intracellular temperature measurements with fluorescent polymeric thermometers. *Chem. Commun.* **2017**, *53*, 10976–10992. [[CrossRef](#)] [[PubMed](#)]
19. Okabe, K.; Inada, N.; Gota, C.; Harada, Y.; Funatsu, T.; Uchiyama, S. Intracellular temperature mapping with a fluorescent polymeric thermometer and fluorescence lifetime imaging microscopy. *Nat. Commun.* **2012**, *3*, 1–9. [[CrossRef](#)] [[PubMed](#)]
20. Cao, S.; Zheng, J.; Zhao, J.; Yang, Z.; Shang, M.; Li, C.; Yang, W.; Fang, X. Robust and Stable Ratiometric Temperature Sensor Based on Zn–In–S Quantum Dots with Intrinsic Dual-Dopant Ion Emissions. *Adv. Funct. Mater.* **2016**, *26*, 7224–7233. [[CrossRef](#)]
21. Haro-González, P.; Martínez-Maestro, L.; Martín, I.R.; García-Solé, J.; Jaque, D. High-sensitivity fluorescence lifetime thermal sensing based on CdTe quantum dots. *Small* **2012**, *8*, 2652–2658. [[CrossRef](#)]
22. Wang, X.; Liu, Q.; Bu, Y.; Liu, C.S.; Liu, T.; Yan, X. Optical temperature sensing of rare-earth ion doped phosphors. *RSC Adv.* **2015**, *5*, 86219–86236. [[CrossRef](#)]

23. Perruchas, S.; Goff, X.F.L.; Maron, S.; Maurin, I.; Guillen, F.; Garcia, A.; Gacoin, T.; Boilot, J.P. Mechanochromic and thermochromic luminescence of a copper iodide cluster. *J. Am. Chem. Soc.* **2010**, *132*, 10967–10969. [[CrossRef](#)] [[PubMed](#)]
24. Lu, D.F.; Hong, Z.F.; Xie, J.; Kong, X.J.; Long, L.S.; Zheng, L.S. High-Nuclearity Lanthanide-Titanium Oxo Clusters as Luminescent Molecular Thermometers with High Quantum Yields. *Inorg. Chem.* **2017**, *56*, 12186–12192. [[CrossRef](#)] [[PubMed](#)]
25. Chen, D.; Liu, S.; Zhou, Y.; Wan, Z.; Huang, P.; Ji, Z. Dual-activator luminescence of RE/TM:Y<sub>3</sub>Al<sub>5</sub>O<sub>12</sub> (RE = Eu<sup>3+</sup>, Tb<sup>3+</sup>, Dy<sup>3+</sup>; TM = Mn<sup>4+</sup>, Cr<sup>3+</sup>) phosphors for self-referencing optical thermometry. *J. Mater. Chem. C* **2016**, *4*, 9044–9051. [[CrossRef](#)]
26. Allison, S.W.; Gillies, G.T. Remote thermometry with thermographic phosphors: Instrumentation and applications. *Rev. Sci. Instrum.* **1997**, *68*, 2615–2650. [[CrossRef](#)]
27. Liu, Y.; Li, C.; Ren, Z.; Yan, S.; Bryce, M.R. All-organic thermally activated delayed fluorescence materials for organic light-emitting diodes. *Nat. Rev. Mater.* **2018**, *3*, 18020. [[CrossRef](#)]
28. Wong, M.Y.; Zysman-Colman, E. Purely Organic Thermally Activated Delayed Fluorescence Materials for Organic Light-Emitting Diodes. *Adv. Mater.* **2017**, *29*, 1605444. [[CrossRef](#)]
29. Fister, J.C.; Rank, D.; Harris, J.M. Delayed Fluorescence Optical Thermometry. *Anal. Chem.* **1995**, *67*, 4269–4275. [[CrossRef](#)]
30. Baleizão, C.; Nagl, S.; Borisov, S.M.; Schäferling, M.; Wolfbeis, O.S.; Berberan-Santos, M.N. An optical thermometer based on the delayed fluorescence of C70. *Chem. A Eur. J.* **2007**, *13*, 3643–3651. [[CrossRef](#)]
31. Liu, J.; Kang, X.; Zhang, H.; Liu, Y.; Wang, C.; Gao, X.; Li, Y. Carbon dot-based nanocomposite: Long-lived thermally activated delayed fluorescence for lifetime thermal sensing. *Dye. Pigment.* **2020**, *181*, 108576. [[CrossRef](#)]
32. Christopherson, C.J.; Mayder, D.M.; Poisson, J.; Paisley, N.R.; Tonge, C.M.; Hudson, Z.M. 1,8-Naphthalimide-Based Polymers Exhibiting Deep-Red Thermally Activated Delayed Fluorescence and Their Application in Ratiometric Temperature Sensing. *ACS Appl. Mater. Interfaces* **2020**, *12*, 20000–20011. [[CrossRef](#)] [[PubMed](#)]
33. Steinegger, A.; Klimant, I.; Borisov, S.M. Purely Organic Dyes with Thermally Activated Delayed Fluorescence—A Versatile Class of Indicators for Optical Temperature Sensing. *Adv. Opt. Mater.* **2017**, *5*, 1700372. [[CrossRef](#)]
34. Zieger, S.E.; Steinegger, A.; Klimant, I.; Borisov, S.M. TADF-Emitting Zn(II)-Benzoporphyrin: An Indicator for Simultaneous Sensing of Oxygen and Temperature. *ACS Sensors* **2020**, *5*, 1020–1027. [[CrossRef](#)] [[PubMed](#)]
35. Zach, P.W.; Freunberger, S.A.; Klimant, I.; Borisov, S.M. Electron-Deficient Near-Infrared Pt(II) and Pd(II) Benzoporphyrins with Dual Phosphorescence and Unusually Efficient Thermally Activated Delayed Fluorescence: First Demonstration of Simultaneous Oxygen and Temperature Sensing with a Single Emitter. *ACS Appl. Mater. Interfaces* **2017**, *9*, 38008–38023. [[CrossRef](#)] [[PubMed](#)]
36. Steinegger, A.; Borisov, S.M. Zn(II) Schiff Bases: Bright TADF Emitters for Self-referenced Decay Time-Based Optical Temperature Sensing. *ACS Omega* **2020**, *5*, 7729–7737. [[CrossRef](#)]
37. Liebsch, G.; Klimant, I.; Wolfbeis, O.S. Luminescence lifetime temperature sensing based on sol-gels and poly(acrylonitrile)s dyed with ruthenium metal-ligand complexes. *Adv. Mater.* **1999**, *11*, 1296–1299. [[CrossRef](#)]
38. Mamada, M.; Fukunaga, T.; Bencheikh, F.; Sandanayaka, A.S.D.; Adachi, C. Low Amplified Spontaneous Emission Threshold from Organic Dyes Based on Bis-stilbene. *Adv. Funct. Mater.* **2018**, *28*, 1–9. [[CrossRef](#)]
39. Malatesta, L.; Angoletta, M. Palladium(0) compounds. Part II. Compounds with triarylphosphines, triaryl phosphites, and triarylarsines. *J. Chem. Soc.* **1957**, 1186–1188. [[CrossRef](#)]
40. Yan, X.; Song, X.; Mu, X.; Wang, Y. Mechanochromic luminescence based on a phthalonitrile-bridging salophen zinc(ii) complex. *New J. Chem.* **2019**, *43*, 15886–15891. [[CrossRef](#)]
41. Xie, D.; Jing, J.; Cai, Y.B.; Tang, J.; Chen, J.J.; Zhang, J.L. Construction of an orthogonal ZnSalen/Salophen library as a colour palette for one- and two-photon live cell imaging. *Chem. Sci.* **2014**, *5*, 2318–2327. [[CrossRef](#)]
42. Cozzi, P.G. Metal-Salen Schiff base complexes in catalysis: Practical aspects. *Chem. Soc. Rev.* **2004**, *33*, 410–421. [[CrossRef](#)] [[PubMed](#)]
43. Im, Y.; Kim, M.; Cho, Y.J.; Seo, J.A.; Yook, K.S.; Lee, J.Y. Molecular Design Strategy of Organic Thermally Activated Delayed Fluorescence Emitters. *Chem. Mater.* **2017**, *29*, 1946–1963. [[CrossRef](#)]
44. Fercher, A.; Borisov, S.M.; Zhdanov, A.V.; Klimant, I.; Papkovsky, D.B. Intracellular O<sub>2</sub> sensing probe based on cell-penetrating phosphorescent nanoparticles. *ACS Nano* **2011**, *5*, 5499–5508. [[CrossRef](#)] [[PubMed](#)]
45. Borisov, S.M.; Mayr, T.; Mistlberger, G.; Waich, K.; Koren, K.; Chojnacki, P.; Klimant, I. Precipitation as a simple and versatile method for preparation of optical nanochemosensors. *Talanta* **2009**, *79*, 1322–1330. [[CrossRef](#)] [[PubMed](#)]
46. Nahidiazar, L.; Agronskaia, A.V.; Broertjes, J.; Van Broek, B.D.; Jalink, K. Optimizing imaging conditions for demanding multi-color super resolution localization microscopy. *PLoS ONE* **2016**, *11*, e0158884. [[CrossRef](#)] [[PubMed](#)]